International Journal of Mechanical, Industrial and Aerospace Sciences
ISSN: 2517-9950
Vol:3, No:11, 2009

# Reconstruction of the Most Energetic Modes in a Fully Developed Turbulent Channel Flow with Density Variation

Elteyeb Eljack, Takashi Ohta

*Abstract*—Proper orthogonal decomposition (POD) is used to reconstruct spatio-temporal data of a fully developed turbulent channel flow with density variation at Reynolds number of 150, based on the friction velocity and the channel half-width, and Prandtl number of 0.71. To apply POD to the fully developed turbulent channel flow with density variation, the flow field (velocities, density, and temperature) is scaled by the corresponding root mean square values ($rms$) so that the flow field becomes dimensionless. A five-vector POD problem is solved numerically. The reconstructed second-order moments of velocity, temperature, and density from POD eigenfunctions compare favorably to the original Direct Numerical Simulation (DNS) data.

*Keywords*—Pattern Recognition, POD, Coherent Structures, Low dimensional modelling.

## I. Introduction

PROPER orthogonal decomposition, also known as Karhunen-Loève expansions in signal processing and pattern recognition, first introduced to turbulence community by Lumley in 1967 as a postprocessing tool for spatio-temporal data obtained from numerical simulation or experimental work. Since then it has been widely used to extract basis functions for reconstruction of coherent structures, low dimensional modelling, and flow control.

The major shortcoming of POD method and its implementation to low dimensional modelling is the dependence of POD basis on the flow parameters and geometry from which they were extracted. However, successful works in kinetic energy analysis, extraction of coherent structures, and low dimensional description of near-wall turbulence are reported continuously. The reader is referred to Lumley [1, 2, 3], Sirovich [4], and Holmes et al. [5] for more details.

In spite of the tremendous efforts to apply POD to turbulent flows, a full three-dimensional POD is applicable to a few types of turbulent flows, e.g., isothermal fully developed boundary layer, channel, pipe, and Couette flow. However, Hasan and Sanghi [6] implemented a method that was explained by Lumley and Poje [7] for flows with density variation. The success of these works inspired us for a further application of POD to a fully developed channel flow with density variation (high density and temperature gradients). The difficulty of applying POD to flows with heat transfer lies in the dimension of the different parameters, i.e., velocity, density, and temperature. Application of POD to the cross-correlation tensor of these parameters would be illogical. Hence, the flow field must be scaled with appropriate parameters to have the same dimension or it becomes dimensionless.

E. Eljack is working as a lecturer in the department of Mechanical Engineering, University of Khartoum, Sudan. Since October 2006 he is doing his PhD at the department of Mechanical Engineering, Osaka University, Yamadaoka, Suita, Osaka, 565-0871, Japan.

T. Ohta is with the department of Mechanical Engineering, Osaka University, Yamadaoka, Suita, Osaka, 565-0871, Japan.

## II. Proper Orthogonal Decomposition

Suppose we have a random velocity field, $u_i(\cdot)$ and we seek to find a deterministic vector field $\phi_i(\cdot)$ which has the maximum projection on our random vector field $u_i$ in a mean square sense. We would like to find a whole new deterministic field represented by $\phi_i(\cdot)$ for which $\overline{|\gamma|^2} = \overline{|u_i(\cdot)\phi_i^*(\cdot)|^2}$ is maximized, i.e.,

$$\overline{|\gamma|^2} = \frac{\overline{(\phi_i(\cdot), u_i(\cdot))^2}}{(\phi_i(\cdot), \phi_i(\cdot))} \tag{1}$$

or

$$\int\int_D R_{ij}(\cdot,\cdot')\phi_i^*(\cdot)\phi_j(\cdot')d(\cdot)d(\cdot') = \lambda \int_D \phi_i(\cdot)\phi_i^*(\cdot)d(\cdot) \tag{2}$$

Where $\lambda = \overline{|\gamma^2|}$. So, if $\phi_i(\cdot)$ maximizes (2), it means that if the flow field is "projected" along $\phi_i(\cdot)$, the average energy content, $\lambda$, is larger than if the flow field is "projected" along any other mathematical structure, e.g. a Fourier mode. In the space orthogonal to this $\phi_i(\cdot)$ the maximization process can be repeated, and in this way a whole set of orthogonal functions $\phi_i(\cdot)$ can be determined. By calculus of variations it can be shown that a necessary condition for $\phi_i(\cdot)$ to maximize expression (2) is that it is a solution of the following Fredholm integral equation of the second type

$$\int_D R_{ij}(\cdot,\cdot')\phi_j(\cdot')d(\cdot') = \lambda\phi_i(\cdot) \tag{3}$$

where, $R_{ij}$ is the space-correlation tensor. This space-correlation tensor is symmetric and positive definite. The power of POD lies in the fact that the decomposition of the flow field in the POD eigenfunctions converge optimally fast in $L^2$-sense. Most importantly, the decomposition is based on the flow field itself; if the flow field is inhomogeneous of finite extent, then Hilbert-Schmidt theory applies and the obtained eigenfunctions are empirical, while if the flow field is homogenous or periodic of infinite extent the eigenfunctions are analytical (sines and cosines). The eigenfunctions of (3) have some interesting mathematical properties. The eigenfunctions are orthogonal as mentioned, and can be normalized; $\left(\phi_i^k(\cdot), \phi_i^l(\cdot)\right) = \delta_{kl}$. The closure of the span of the POD

eigenfunctions is equal to the set of all realizable flow fields. Thus, the original velocity field can be reconstructed from them as follows:

$$u_i(\cdot) = \sum_{n=0}^{\infty} a_n \phi_i^n(\cdot) \tag{4}$$

The random coefficients $a_n$ are functions of the variables not used in the integral, and must be determined by projection back onto the velocity field i.e.,

$$a_n = \int_D u_i(\cdot)\phi_j^{*n}(\cdot)d(\cdot) \tag{5}$$

They are uncorrelated and their mean values are the eigenvalues $\lambda$

$$\lambda_n = \overline{a_n a_m}\delta_{nm} \tag{6}$$

The eigenvalues are ordered (meaning that the lowest order eigenvalue is bigger than the next, and so on); i.e, $\lambda_1 > \lambda_2 > \lambda_3 \cdots$. Thus, the representation is optimal in the sense that the fewest number of terms is required to capture the energy.

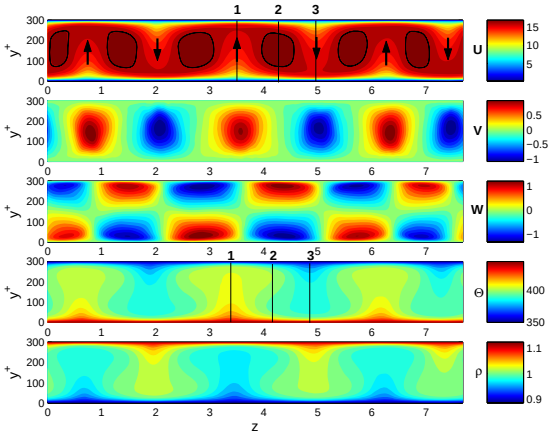


Fig. 1. Contour plot of stream-wise mean velocity $U$, wall-normal mean velocity $V$, cross-stream mean velocity $W$, mean temperature $\Theta$, and mean density $\rho$. The arrows on $U$ contour plot show the direction of rotation of the Rayleigh-Benard counter-rotating vortices. The color bars to the right show the magnitude of the contours.

## III. Flow fields with density variation

In many interesting practical flows, temperature fluctuations contribute to the generation of velocity fluctuations and turbulent kinetic energy. Temperature fluctuations cause density fluctuations in the fluid at essentially constant pressure. The density fluctuations cause a fluctuating body force which contribute to the turbulent kinetic energy. To construct an optimal representation for such flows using empirical eigenfunctions, vector and scalar fields must be scaled with appropriate parameters so that they have the same dimension or they become dimensionless. A five-vector maximization problem is formulated as follows:

$$\overline{|\alpha|^2} = \frac{\overline{(\varphi_i(\cdot), \upsilon_i(\cdot))^2}}{(\varphi_i(\cdot), \varphi_i(\cdot))} \tag{7}$$

Where, $\varphi_i(\cdot)$ are empirical candidate eigenfunctions and $\upsilon_i(\cdot)$ are scaled vector and scalar quantities, i.e., $\frac{u}{u_{rms}}$, $\frac{v}{v_{rms}}$, $\frac{w}{w_{rms}}$, $\frac{\varrho}{\varrho_{rms}}$, and $\frac{\theta}{\theta_{rms}}$.

## IV. POD of the channel flow with density variation

The flow field simulated is a fully developed turbulent flow between two parallel walls. The walls are assumed to be kept at different but constant temperatures without fluctuations. The lower wall is hot and the upper one is cold. The flow is driven by a constant pressure gradient in the stream-wise direction and buoyancy forces in the wall-normal direction. The flow field is periodic in the stream-wise direction and statistics are dependent on the cross-stream and wall-normal directions. The governing equations are the compressible Navier-Stokes equations, continuity equation, energy equation, and the equation of state for ideal gas. These equations were non-dimensionalized using characteristic scales of each variable. The fluid is assumed to be air and its viscosity, $\mu$, varies with temperature according to Sutherland equation, Thermal conductivity, $k$, is obtained from viscosity using Eucken equation. A new method linking the pressure and density was used. A second order central difference method was used for the spatial derivative. The fractional method is applied for time evolution, which is based on the second order Adams-Bashforth method for convection and diffusion terms and implicit backward Euler method for the continuity equation and pressure term. The computational domain was chosen to be $15.84 \times 1 \times 7.68$ and divided into $256 \times 128 \times 256$ grid points in the stream-wise, wall-normal, and cross-stream directions, respectively. Periodic boundary conditions were applied in the stream-wise direction and non-slip boundary condition was used on the walls. Simulation parameters are as follows; Reynolds number $Re_\tau = 150$, Prandtl number $Pr = 0.71$, the hot wall temperature $\Theta_h = 450$, and the cold wall temperature $\Theta_c = 350$. The results were compared to those of the Boussinesq approximation. Ohta et al. [8], and Ohta et al. [9].

Figure 1 shows a contour plot of $U$, $V$, $W$, $\Theta$, and $\rho$. To improve the time averaged values, all statistics were averaged over the stream-wise direction (homogenous direction). The dominating coherent structures of the mean flow are counter rotating vortices of the size of the channel width. These counter rotating vortices are driven by the Rayleigh-Benard convection between the two walls, and they do not have fluctuating part. Figure 2 show the stream-wise mean velocity component at three different cross-stream positions. The wall-normal mean velocity component, $V$, convects the flow in the directions shown by the arrows in figure 1. The cross-stream mean velocity component, $W$, advects the flow in the cross-stream direction from regions of positive values of $W$ to regions of negative values. Advection by the cross-stream mean velocity component considerably affects the profile of mean temperature and density profiles. The mean temperature, $\Theta$, decreases monotonically at positions 1 and 3. But, it has a non-monotonic profile at position 2 due to horizontal advection by $W$ as shown in figure 3. Positions 1,2, and 3 are marked by lines in figure 1 on $U$ and $\Theta$ contours.

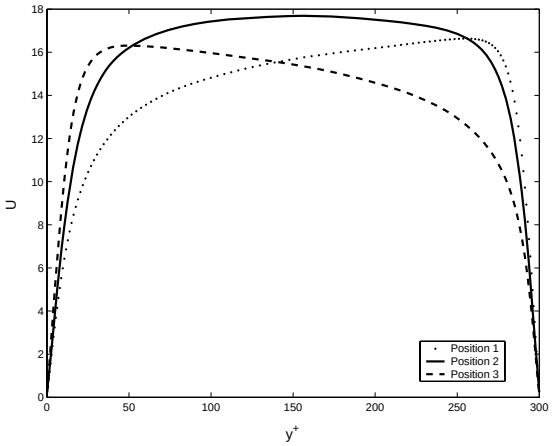


Fig. 2. Mean velocity profile at cross-stream positions 1, 2, and 3

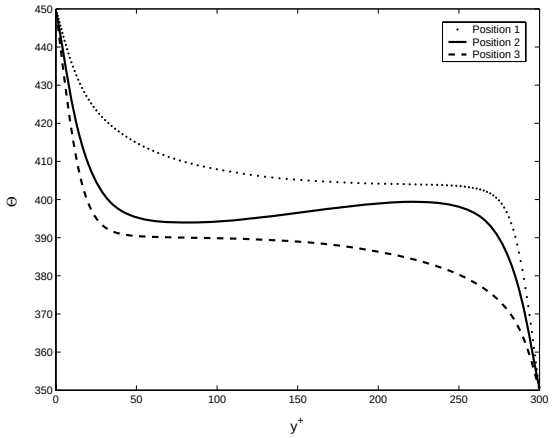


Fig. 3. Mean temperature profile at cross-stream positions 1, 2, and 3

We wish to construct a representation of this flow using empirical eigenfunctions. We have a random velocity, temperature and density fields; $u_i(\cdot)$, $\theta(\cdot)$ and $\varrho(\cdot)$, respectively. We seek to find a deterministic vector field $\varphi_i(\cdot)$ that has the maximum projection on our random fields in a mean square sense. We would like to find a whole new deterministic fields represented by $\varphi_i(\cdot)$ for which $\overline{|\varepsilon_i|^2} = \overline{|\upsilon_i(\cdot)\varphi_i^*(\cdot)|^2}$ are maximized. Due to dimensional consideration, vector and scalar fields can not be included in one maximization problem. Alternatively, vector fields and scalar fields can be maximized separately as follows:

$$\overline{|\gamma|^2} = \frac{\overline{(\varphi_i(\cdot), u_i(\cdot))^2}}{(\varphi_i(\cdot), \varphi_i(\cdot))} \tag{8}$$

$$\overline{|\gamma_\varrho|^2} = \frac{\overline{(\varphi_4(\cdot), \varrho(\cdot))^2}}{(\varphi_4(\cdot), \varphi_4(\cdot))} \tag{9}$$

$$\overline{|\gamma_\theta|^2} = \frac{\overline{(\varphi_5(\cdot), \theta(\cdot))^2}}{(\varphi_5(\cdot), \varphi_5(\cdot))} \tag{10}$$

In the above approach, the cross-correlation between vector fields and scalar fields is not considered. Hence, a better approach would be to define a five-vector maximization problem using the three velocity components, temperature and density fluctuations. In order to do this in a rational manner, we need to normalize the various components in such a way that they all have the same dimension. This raises the question of scaling; what are the best parameters to scale the five components, $u_i(\cdot)$, $\theta(\cdot)$, and $\varrho(\cdot)$ ? There are two ways to do this; either scaling the various components of the raw data or scaling the cross-correlation tensor. [6] and [7] scaled the two point cross correlation tensor with the root mean square of the stream-wise velocity fluctuation ($u_{rms}$) and the root mean square of density fluctuation ($\varrho_{rms}$). However, in this study the flow field is scaled with the root mean square value of each component, i.e., $u^s = \frac{u}{u_{rms}}$, $v^s = \frac{v}{v_{rms}}$, $w^s = \frac{w}{w_{rms}}$, $\varrho^s = \frac{\varrho}{\varrho_{rms}}$, and $\theta^s = \frac{\theta}{\theta_{rms}}$. This way the flow field becomes dimensionless. Hence, the use of a five vector maximization problem is straightforward,

$$\int\int_D R_{ij}^s(\cdot,\cdot')\psi_i^*(\cdot)\psi_j(\cdot')d(\cdot)d(\cdot') = \Lambda\int_D \psi_i(\cdot)\psi_i^*(\cdot)d(\cdot) \tag{11}$$

And $\psi_i(\cdot)$ is a solution of the following Fredholm integral equation:

$$\int_D R_{ij}^s(\cdot,\cdot')\psi_j(\cdot')d(\cdot') = \Lambda\psi_i(\cdot) \tag{12}$$

The flow is homogenous in the stream-wise direction, $x$, and inhomogeneous bounded in the wall-normal direction. The fluctuating velocities, temperature, and density can be treated as homogenous signals in the cross-stream direction, that is, the two-point correlations are independent in origin in space in this direction, at leat for such a low Reynolds number. Fourier transforming equations (12) in $x$ and $z$ directions, space correlation tensor $R_{ij}^s(x,x',y,y',z,z')$ becomes cross spectra tensor $S_{ij}^s(y,y';k_1,k_3)$ and equations (12) can be rewritten as follows:

$$\int_D S_{ij_{k_1k_3}}^s(y,y')\psi_{j_{k_1k_3}}(y')dy' = \Lambda_{k_1k_3}\psi_{i_{k_1k_3}}(y) \tag{13}$$

Equation (13) can be formulated as an eigenvalue problem, again trapezoidal rule with up to $N = 65$ non-uniformly spaced grid points from one wall to the channel center line was used to approximate the integral:

$$A_{ij_{k_1k_3}}^s\psi_{j_{k_1k_3}} = \Lambda_{k_1k_3}\psi_{i_{k_1k_3}} \tag{14}$$

For 3 dimensions ($x$, $y$, and $z$), 3 velocity components ($u^s$, $v^s$, and $w^s$), density ($\varrho^s$) and temperature ($\theta^s$) the above equations can be rewritten in matrix form as follows:

$$\begin{pmatrix} A_{11}^s & A_{12}^s & \cdots & A_{15}^s \\ A_{21}^s & A_{22}^s & \cdots & A_{15}^s \\ A_{31}^s & A_{32}^s & \cdots & A_{15}^s \\ A_{41}^s & A_{42}^s & \cdots & A_{45}^s \\ A_{51}^s & A_{52}^s & \cdots & A_{55}^s \end{pmatrix} \begin{pmatrix} \psi_1 \\ \psi_2 \\ \psi_3 \\ \psi_4 \\ \psi_5 \end{pmatrix} = \Lambda \begin{pmatrix} \psi_1 \\ \psi_2 \\ \psi_3 \\ \psi_4 \\ \psi_5 \end{pmatrix} \tag{15}$$

POD integration domain was chosen to be equivalent to that of a channel in minimal flow unit with the following grid distribution; $(256\times65\times32)$. Solving these equations numerically for each pair of wave numbers $\left(k_1 = \frac{2\pi m}{L_x}, k_3 = \frac{2\pi l}{L_z}\right)$ yields POD basis $\psi_1$, $\psi_2$, $\psi_3$, $\psi_4$ and $\psi_5$ and eigenspectra $\Lambda$.

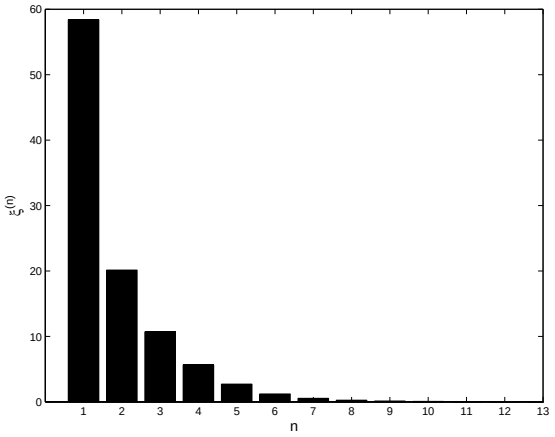


Fig. 4. Kinetic energy distribution among POD modes.

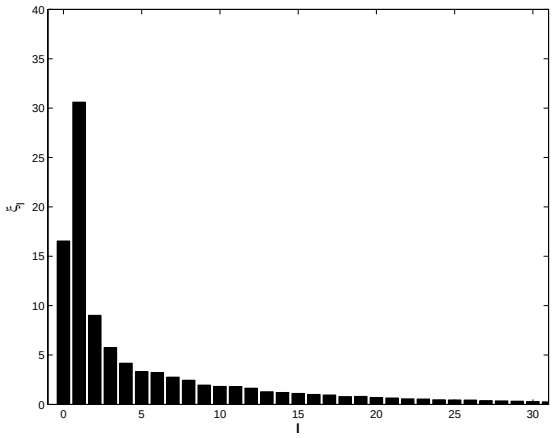


Fig. 5. Kinetic energy distribution among cross-stream modes.

### A. Kinetic Energy:

The total kinetic energy $\xi_t$ is the sum over all POD modes, stream-wise modes and cross-stream modes.

$$\xi_t = \sum_n \sum_m \sum_l \Lambda_{ml}^{(n)} \tag{16}$$

from which, energy percentage as a function of wall-normal mode index $n$ and cross-stream mode index $l$ is given by:

$$\xi^{(n)} = \frac{\sum_m \sum_l \Lambda_{ml}^{(n)}}{\sum_n \sum_m \sum_l \Lambda_{ml}^{(n)}}; \quad \xi_l = \frac{\sum_n \sum_m \Lambda_{ml}^{(n)}}{\sum_n \sum_m \sum_l \Lambda_{ml}^{(n)}} \tag{17}$$

Figure 4 shows the kinetic energy distribution among the first 13 POD modes. Consistent with previous studies, POD mode 1, 2, and 3 contain about 60%, 20%, and 10%, respectively, of the total kinetic energy. Figure 5 shows the kinetic energy distribution among the first 32 cross-stream modes. Cross-stream mode two is the most energetic mode and the eigenspectra peaks at off-origin location indicating a recurrence of coherent structures in this direction.

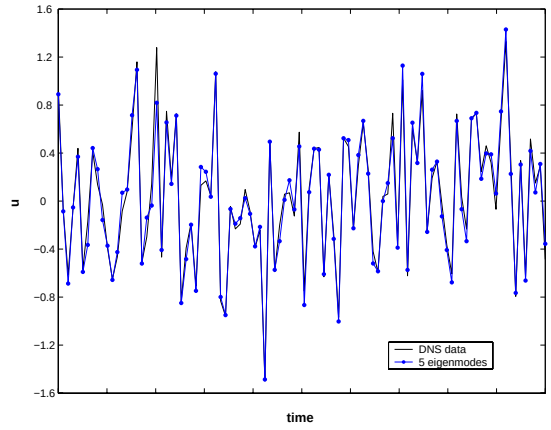


Fig. 6. Convergence of POD modes, contribution of 5 eigenmodes to $u$.

### B. Reconstruction of the instantaneous velocity field

To understand how the POD represents the original velocity, temperature, and density signal, the instantaneous fields were reconstructed. The doubly Fourier transformed random velocity, temperature, and density, $\hat{\hat{u}}_{ik_1k_3}(y,t)$, $\hat{\hat{\theta}}_{k_1k_3}(y,t)$, and $\hat{\hat{\varrho}}_{k_1k_3}(y,t)$, can be reconstructed from the eigenfunctions as follows:

$$\hat{\hat{u}}_{ik_1k_3}(y,t) = u_{irms} \sum_{n=1}^{\infty} a_{k_1k_3}^{(n)}(t) \psi_{ik_1k_3}^{(n)}(y) \tag{18}$$

$$\hat{\hat{\theta}}_{k_1k_3}(y,t) = \theta_{rms} \sum_{n=1}^{\infty} a_{k_1k_3}^{(n)}(t) \psi_{5k_1k_3}^{(n)}(y) \tag{19}$$

$$\hat{\hat{\varrho}}_{k_1k_3}(y,t) = \varrho_{rms} \sum_{n=1}^{\infty} a_{k_1k_3}^{(n)}(t) \psi_{4k_1k_3}^{(n)}(y) \tag{20}$$

And consequently, the Reynolds stresses, heat fluxes, and density fluxes are given by

$$\overline{u_i u_j} = u_{irms} u_{j\,rms} \sum_n \sum_m \sum_l \Lambda_{ml}^{(n)} \psi_{iml}^{(n)}(y) \psi_{jml}^{(n)*}(y) \tag{21}$$

$$\overline{u_i \theta} = u_{irms} \theta_{rms} \sum_n \sum_m \sum_l \Lambda_{ml}^{(n)} \psi_{iml}^{(n)}(y) \psi_{5ml}^{(n)*}(y) \tag{22}$$

$$\overline{\varrho u_i} = \varrho_{rms} u_{irms} \sum_n \sum_m \sum_l \Lambda_{ml}^{(n)} \psi_{iml}^{(n)}(y) \psi_{4ml}^{(n)*}(y) \tag{23}$$

Figures 6 and 7 show how the reconstructed instantaneous stream-wise velocity signal compare to the original data in time and space. In both cases, five eigenmodes represents the original signal favorably. Figures 8, 9, 10, 11, and 12 show the reconstruction of $u_{rms}$, $v_{rms}$, $w_{rms}$, $\theta_{rms}$ and $\rho_{rms}$ using 1, 2, 3, 4, and 5 POD eigenmodes. POD representation of the flow field converges rapidly to the corresponding DNS data.

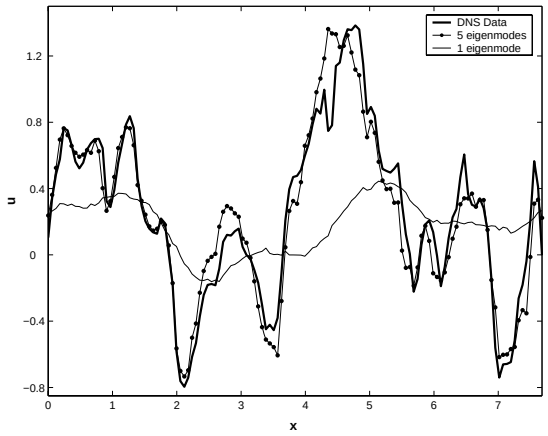


Fig. 7. Convergence of POD modes, contribution of 1 and 5 eigenmodes to $u$.

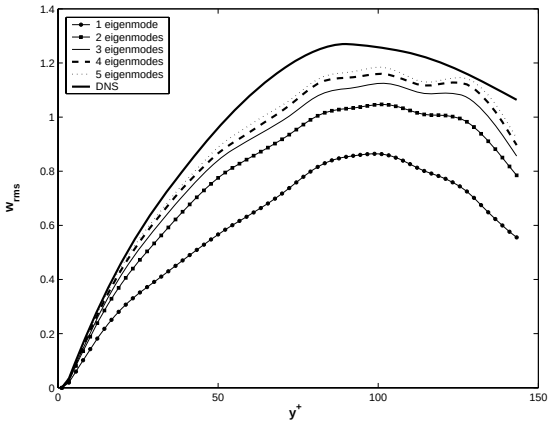


Fig. 10. Convergence of POD modes, contribution of 1, 2, 3, 4, and 5 eigenmodes to $w_{rms}$.

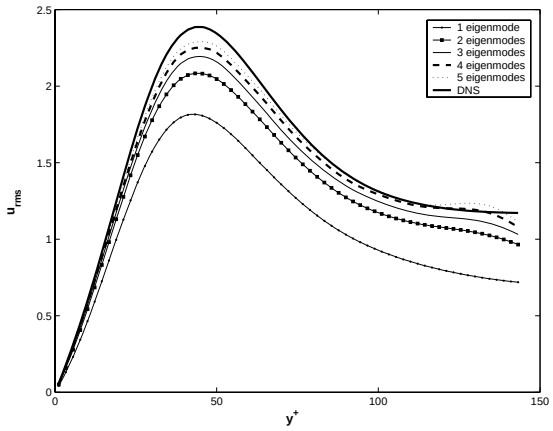


Fig. 8. Convergence of POD modes, contribution of 1, 2, 3, 4, and 5 eigenmodes to $u_{rms}$.

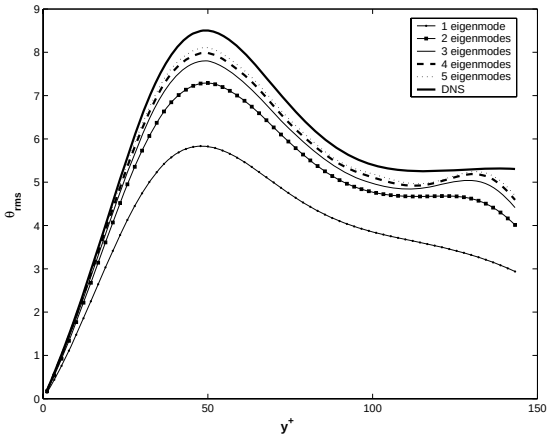


Fig. 11. Convergence of POD modes, contribution of 1, 2, 3, 4, and 5 eigenmodes to $\theta_{rms}$.

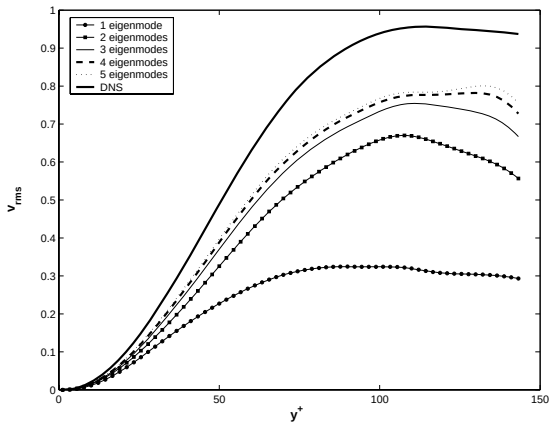


Fig. 9. Convergence of POD modes, contribution of 1, 2, 3, 4, and 5 eigenmodes to $v_{rms}$.

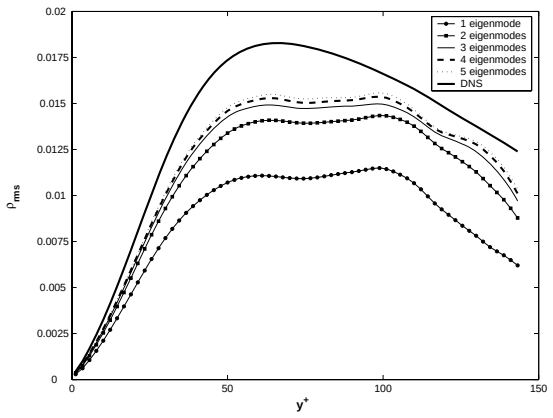


Fig. 12. Convergence of POD modes, contribution of 1, 2, 3, 4, and 5 eigenmodes to $\rho_{rms}$.

## V. Conclusion

A five-vector POD eigenvalue problem was developed to include the cross-correlation of velocities, density, and temperature. This way the POD maximizes the total energy including effects of temperature and density. Since applying POD to the cross-correlation or cross-spectra tensor of parameters with different dimensions would be illogical, the flow field therefore must be scaled with appropriate parameters to have the same dimension or it becomes dimensionless. We have scaled the raw data with the corresponding root mean square values. The contribution from lower modes (big structures) and higher modes (small structures) to the normal stresses is always positive and POD mode 1, 2, and 3 contain about $60\%$, $20\%$, and $10\%$, respectively, of total kinetic energy. Five eigenmodes reconstruction of second-order moment of velocity, temperature and density converge rapidly to the original DNS data.

## Acknowledgment

Financial support by the Japanese Ministry of Education, Culture, Sports, Science and Technology (MEXT) is highly acknowledged.

## References

[1] Lumley, J. L. (1967) The Structure of Inhomogeneous Turbulent Flows. In Atmospheric Turbulence and Radio Wave Propagation (A.M. Yaglom and V.I. Takarski, eds.), pp. 166–178. Moscow: Nauka.

[2] Lumley, J. L. (1972) Stochastic Tools in Turbulence. New York: Academic Press.

[3] Lumley, J. L. (1981) Coherent Structures in Turbulence. In Transition and Turbulence (R.E. Meyer, ed.), pp. 215-242. New York: Academic Press.

[4] Sirovich, L. (1987) Turbulence and the Dynamics of Coherent Structures, parts I-III., Q. Appl. Maths XLV (3), pp. 561–590.

[5] Holmes, P. Lumley, J. L. and Berkooz, G. (1996) Turbulence, Coherent Structures, Dynamical Systems and Symmetry, Cambridge University Press.

[6] Hasan Nadeem and Sanghi Sanjeev (2007) Proper Orthogonal Decomposition and Low-dimensional Modelling of Thermally Driven Two-dimensional Flow in a Horizontal Rotating Cylinder, J. Fluid Mech. Vol. 573, pp. 265–295.

[7] Lumley, J. L. and Poje, A. (1997) Low-dimensional Models for Flows with Density Fluctuations, Phys. Fluids 9, pp. 2023–2031.

[8] Ohta, T. Mizobata, K. and Kajishima, T. (2006) Influence of Density Fluctuation on DNS of Turbulent Channel Flow in The Presence of Temperature Stratification, In Proc. of The $5^{th}$ Int. Symp. on Turbulence, Heat and Mass Transfer - Dubrovnik, Croatia, September 25-29.

[9] Ohta, T. Nakamura, K. Mizobata, K. and Kajishima, T. (2007) DNS of Turbulent Channel Flow with Density Variation Under Some Conditions of Unstable Stratification, In Proc. of HT2007 ASME-JSME Thermal Engineering Summer Heat Transfer Conference, July 8-12, Vancouver, British Columbia, Canada.

## Nomenclature

| | |
|---|---|
| $\delta_{i,j}$ | Kronecker delta |
| $\theta$ | temperature fluctuation |
| $\Theta$ | mean temperature |
| $\lambda$ | eigenvalue |
| $\Lambda$ | eigenvalue |
| $\nu$ | viscosity |
| $\varrho$ | density fluctuation |
| $\rho$ | mean density |
| $\phi_i$ | $i$ eigenfunction component |
| $\Phi$ | eigenfunction vector |
| $\psi_i$ | $i$ eigenfunction component |
| $\Psi$ | eigenfunction vector |
| $\hat{a}$ | Fourier transform of $a$ |
| $\overline{a}$ | ensemble average of $a$ |
| $a_n$ | POD coefficient |
| D | Domain |
| h | channel half-width |
| $k_1, k_3$ | stream-wise, cross-stream wave numbers |
| $l$ | cross-stream mode |
| $L_x, L_z$ | size of space domain in $x, z$ directions |
| $m$ | stream-wise mode |
| n | POD mode (wall-normal mode) |
| N | number of data points in $y$ direction |
| rms | root mean square |
| $Re_\tau$ | Reynolds number = $\frac{u_* h}{\nu}$ |
| $R_{ij}$ | space correlation tensor |
| $S_{ij}$ | cross-spectra tensor |
| $u_i$ | $i$ velocity fluctuation component |
| $u_*$ | friction velocity |
| $(\cdot, \cdot')$ | inner product |